Original Research

Investigation of Lanthanide-Based Starch Particles as a Model System for Liver Contrast Agents

Sigrid L. Fossheim,[1] Kenneth E. Kellar,[2] Sven Månsson,[3] Jean-Marie Colet,[4] Pål Rongved,[5] Anne Kjersti Fahlvik,[5] and Jo Klaveness[1]

Gadolinium and dysprosium diethylenetriamine pentaacetic acid-labeled starch microparticles (Gd-DTPA-SP and Dy-DTPA-SP) were investigated as model liver contrast agents. The liver contrast efficacy of particles with low and high metal contents was compared in two imaging models: in vivo rat liver and ex vivo perfused rat liver. The biodistribution of intravenously injected particles was also assessed by ex vivo relaxometry and inductively coupled plasma atomic emission spectrophotometry of tissues. All particles reduced the liver signal intensity on T2-weighted spin-echo and gradient-recalled echo images as a result of susceptibility effects. Because of their higher magnetic susceptibility, the Dy-DTPA-SP were more effective negative contrast enhancers than the Gd-DTPA-SP. On T1-weighted spin-echo images, only the Gd-DTPA-SP with low metal content significantly increased the liver signal intensity. In addition, these low-loading Gd-DTPA-SP markedly reduced the blood T1. The two latter observations were not consistent with the anticipated blood circulation time of microparticles, but were a result of the lower stability of these particles in blood compared with Gd-DTPA-SP, which has a high metal content. Regardless of stability or imaging conditions, the paramagnetic starch particles investigated showed potential as negative liver contrast enhancers. However, the observed accumulation of particles in the lungs represented a biological limitation for their use as contrast agents. J. Magn. Reson. Imaging 1999; 9:295–303. © **1999 Wiley-Liss, Inc.**

Index terms: starch particles; dysprosium; gadolinium; liver contrast efficacy; susceptibility effects

Abbreviations: FOV = field of view; Gd = Gadolinium; GRE = gradient recalled echo; Dy = dysprosium; DTPA = diethylenetriamine pentaacetic acid; ICP-AES = inductively coupled plasma atomic emission spectrophotometry; MPS = mononuclear phagocyte system; RCE = relative contrast enhancement; ROI = region of interest; SE = spin echo; SEM = standard error of the mean; SI = signal intensity; SNR = signal-to- noise-ratio; SP = starch particle; SRR = signal-to-reference ratio; TE = echo time; TR = repetition time.

[1]Department of Medicinal Chemistry, School of Pharmacy, University of Oslo, 0316 Oslo, Norway.

[2]Nycomed Amersham Imaging, 466 Devon Park Drive, PO Box 6630, Wayne, Pennsylvania.

[3]Department of Experimental Research, Malmø University Hospital, University of Lund, Malmø, Sweden.

[4]NMR Laboratory, Department of Organic Chemistry, University of Mons-Hainaut, 24 Avenue du Champs de Mars, B-7000 Mons, Belgium.

[5]Nycomed Imaging AS, PO Box 4220, Torshov N-401 Oslo, Norway.

Contract grant sponsor: Norwegian Research Council; Contract grant number: 107462/410; Contract grant sponsor: ARC Program of the French Community of Belgium; Contract grant number: 95/00–194.

Address reprint requests to: S.L.F., Department of Medicinal Chemistry, School of Pharmacy, University of Oslo, P.O. Box 1155 Blindern, 0316 Oslo, Norway.

Received February 2, 1998; Accepted March 25, 1998.

PARAMAGNETIC PARTICULATE MATERIALS, such as liposomal gadolinium (Gd) formulations and manganese hydroxyapatite, have been extensively investigated as potential organ-specific contrast agents for magnetic resonance imaging (MRI) (1–3). Most research on paramagnetic particles has focused on their ability to enhance contrast by functioning as positive (T1) contrast agents; their potential as negative (T2) contrast agents has been discussed only in the case of manganese carbonate particles (4). However, water-soluble low-molecular-weight (Gd) and dysprosium (Dy) chelates have been shown to function as negative contrast agents for cerebral and cardiac imaging (5–7). Unless extremely high concentrations of the chelates are used, the negative contrast effect arises from a compartmentation of the agent. In a magnetic field, the compartment containing the agent can be regarded as a large "magnetic particle" to extracompartmental water protons, and T2 is shortened as a result of water protons diffusing in the outer-sphere environment of the magnetized compartment. This relaxation enhancement is often referred to as the susceptibility effect (8).

In the present work, the ability of starch particles, containing covalently linked Gd- and Dy-diethylenetriamine pentaacetic acid (Gd-DTPA and Dy-DTPA), to function as positive and negative liver contrast agents was evaluated. The contrast efficacy of particles with low and high metal contents was compared in a variety of ex vivo and in vivo liver models. The biodistribution of intravenously injected particles was assessed by inductively coupled plasma atomic emission spectrophotometry and by relaxation analyses of excised tissues and withdrawn blood.

MATERIALS AND METHODS

Particulate Substances

The starch particles consisted of epichlorohydrin cross-linked hydrolyzed potato starch labeled with Gd-DTPA or Dy-DTPA, referred to as Gd-DTPA-SP and Dy-DTPA-SP, respectively (Fig. 1) (9). Because of the swellable nature of the particle, the labeling procedure ensured that metal chelate was located homogeneously through-

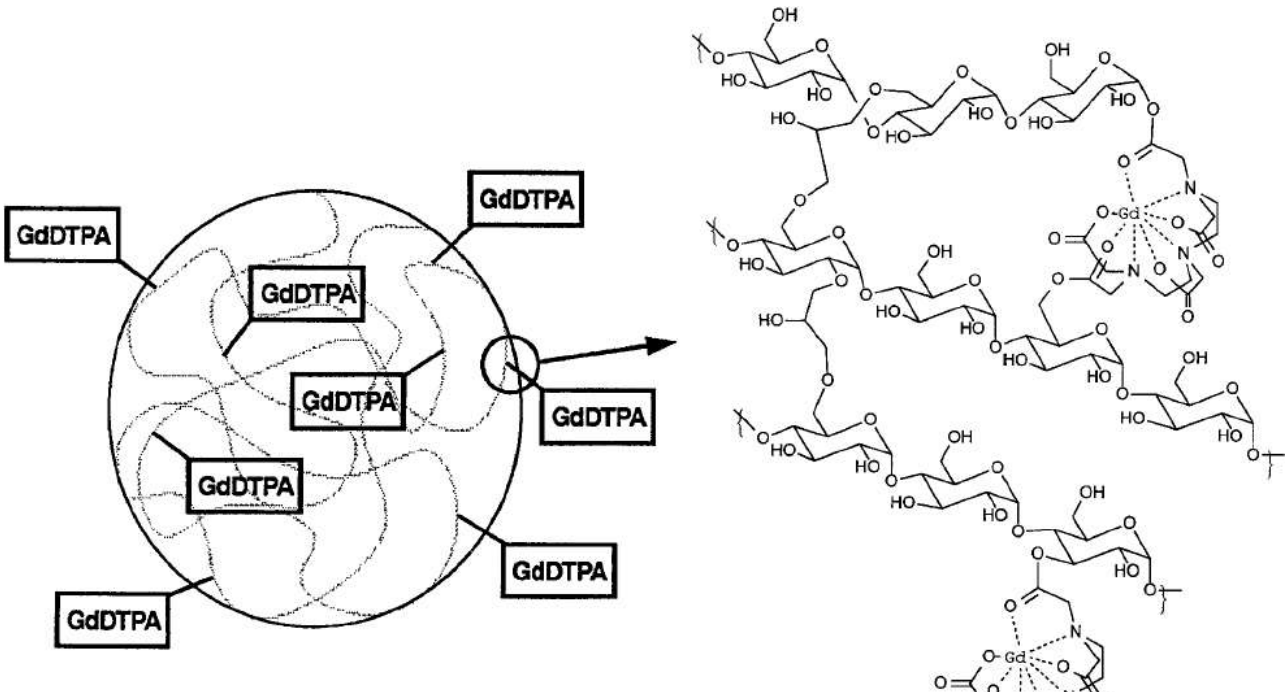

Figure 1. Anticipated structure of Gd-DTPA-SP and Dy-DTPA-SP.

out the particle, including the surface (9,10). Particulate formulations with varying metal contents were prepared and lyophilized until further use (Virtis Benchtop Lyophilisator BT-5L, Virtiscomp, Gordimer, NJ).

Particle Characterization

The metal content of the particles was determined by inductively coupled plasma atomic emission spectrophotometry (ICP-AES) (11). For the Dy-DTPA-SP, the Dy content varied from 2.7% to 12.7% (w/ w), and the Gd content of the Gd-DTPA-SP ranged from 2.7% to 9.3%. For particle size and electrophoretic mobility analyses, particles were suspended in an isotonic 5% (w/ v) glucose solution (Glucose 50 mg/ ml, B. Braun, AG Melsungen, Germany), sonicated, and filtered through 5-µm filters (Millex-SV, Millipore, Bedford, MA). The mean volume-weighted particle diameter was determined by the Coulter counter technique (Coulter Counter Multi-Sizer II, Coulter Electronics, Luton, England). Electrophoretic mobility was measured by laser Doppler velocimetry (Delsa 440, Coulter Electronics, and ZetaSizer IV, Malvern Instruments, Malvern, England).

Magnetic Characterization

The magnetic properties of particles with 2.7% metal content have previously been determined by variable-temperature vibrating sample magnetometry (11). The magnetic susceptibilities of the Dy-DTPA-SP and Gd-DTPA-SP at 22°C were 4.9 and $2.4 \cdot 10^{-2}$ cm^3 mol^{-1}, respectively. The magnetic measurements of the particulate substances with higher metal content were performed on a vibrating sample magnetometer operating at 22°C (Molspin, Newcastle upon Tyne, England). The magnetization was recorded in the field strength range from -1 to 1 T and was corrected for diamagnetic contributions (sample container and particle starch matrix). The slope of the corrected magnetization versus field strength curve was obtained by a linear least-squares regression analysis from which the magnetic susceptibility was calculated (11).

In Vitro Relaxometry

Particles were suspended in 0.8% (w/ v) agar gel (Agar, Kebo Lab, Oslo, Norway) to prevent aggregation and sedimentation during the time course of the relaxation measurements. The sonicated and filtered aqueous particulate suspension, prepared as previously described, was shaken horizontally (HS 500, Janke & Kunkel, Staufen i. Breisgau, Germany) with a heated agar solution. Relaxometry was performed at 37°C and 0.47 T (Minispec PC-120b, Bruker, Rheinstetten, Germany). T1 relaxation times were obtained by the inversion recovery method, and T2 relaxation times were determined from a Carr-Purcell-Meiboom-Gill spin-echo (SE) pulse sequence with an echo time (TE) of 4 msec. The T1 and T2 relaxivities (r1 and r2 respectively) were obtained from a linear least-squares regression analysis of relaxation rate (1/ T1, 1/ T2) versus metal ion concentration. For comparative and control purposes, the relaxivities of Gd-DTPA (Magnevist, Schering, Berlin, Germany) and Dy-DTPA (prepared from $DyCl_3$ and DTPA) were also determined in 0.8% agar gel. The metal

ion concentration in agar samples was determined by ICP-AES.

Ex Vivo Tissue Relaxometry

Particles with 2.7% metal content were dispersed in a 5% glucose solution, as previously described[1], and administered iv to male Wistar rats (Møllegaard Breeding Center, Ejby, Denmark) at dosages of 20, 50, and 150 µmol Gd or Dy/ kg body weight ($n = 4$). The injection volume was 1.6 mL/ 100 g, and the injection rate was 0.5 mL/ min. A volume equivalent injection of a 5% glucose solution was administered iv to control rats ($n = 10$). The rats were anesthetized 30 minutes after injection by an intraperitoneal injection of pentobarbital. The rats were laparotomized, and blood was taken from the vena cava. The latter was then severed to effect euthanasia. T1 and T2 of liver, spleen, and lungs were measured at 37°C and 0.47 T within 2 hours of tissue excision and were also recorded in homogenized liver (Ika Werk TP 18–10 homogenizator, Ika Werk, Staufen i. Breisgau, Germany). The T1 and T2 of blood were measured within 10 minutes of withdrawal. The apparatus and pulse sequence parameters were analogous to those used for the in vitro relaxometry.

In Vivo Liver Imaging

Liver imaging was performed at 2.4 T (Biospec 24/ 30, Bruker, Ettlingen, Germany). Male Wistar rats (Møllegaard Breeding Center, Ejby, Denmark) were anesthetized by intraperitoneal administration of pentobarbital. Particulate formulations with low (2.7% Gd or Dy) and high (9.3% Gd or 10.9% Dy) metal contents were prepared as previously described[1] and administered iv to rats. Dosages of 20, 50, 100, and 150 µmol Gd or Dy/ kg body weight were used for the low-loading particles ($n = 3$). Rats received injections of the high-loading particles at dosages of 50 and 100 µmol Gd or Dy/ kg body weight ($n = 3$). The injection volume was 1.6 or 1.0 mL/ 100 g for the low-loading particles and high-loading particles, respectively, and the injection rate was 0.5 mL/ min. A volume equivalent injection of a 5% glucose solution was given iv to the control rats ($n = 6$ or 8). Groups of one control and three test rats were imaged at each dosage.

T2*-weighted (T2*-w) gradient-recalled echo (GRE) and T1-w SE axial images of the liver were obtained 15 and/ or 30 minutes after injection. The following pulse sequence parameters were used for the particles with low metal content: T1-w SE: TR/ TE 150/ 12.6 msec; GRE: TR/ TE/ flip angle = 50/ 14 msec/ 20°. Modified parameters were employed for particles with high metal content: T1-w SE: TR/ TE 157/ 13.5 msec; GRE: TR/ TE/ flip angle 80/ 9 msec/ 20°. The T1-w SE pulse sequences were considered equal. To minimize susceptibility artifacts, the GRE sequence used for the high-loading particles required a significantly shorter TE. Consequently, the GRE sequences could not be directly compared. The following parameters were fixed for all experiments: field of view (FOV) 12 cm; matrix size 256 × 256; number of slices 3; slice thickness 5 mm. The third slice was selected for image analysis. The mean signal intensity of liver (SI_{liver}) was measured within a freehand-drawn region of interest (ROI) in the liver parenchyma. For background noise, the mean signal intensity (SI_{noise}) was measured within a large circular ROI, located in an area not disturbed by motion artifacts. The percentage relative contrast enhancement (RCE) in the liver parenchyma was calculated as: $RCE = 100 \times (SNR_{test} - SNR_{control}) / SNR_{control}$, where SNR_{test} is the signal-to-noise ratio, SI_{liver}/ SI_{noise}, for test rats, and $SNR_{control}$ is the mean SNR of the control group.[2] The rats were sacrificed by intraperitoneal injection of pentobarbital. Lungs, spleen, and liver were excised, weighed, and freeze-stored for later ICP-AES analysis.

Ex Vivo Liver Imaging

The contrast efficacy of particles with high metal content (8.0% Gd or 9.6% Dy) was assessed in the isolated and perfused rat liver at 4.7 T (MSL-200–15, Bruker, Rheinstetten, Germany). Livers were isolated from anesthetized male Wistar rats (Iffa Credo, Brussels, Belgium) and perfused at 37°C with a constant flow (3–4 mL/ min/ g of liver) through the portal vein with about 200 mL of a recirculating Krebs-Henseleit buffer (containing no EDTA) saturated with carbogen (95% O_2, 5% CO_2) (12,13). The particulate preparations (1.6 mL/ 100 g) were added to the perfusion fluid at a rate of 0.8 mL/ min and at a dosage of 150 µmol Gd or Dy/ kg body weight ($n = 3$). After 60 minutes of recirculatory perfusion, the livers were perfused for 30 minutes in the nonrecirculating mode to wash out the extracellular space of liver. T2-w SE axial images of the liver were acquired with: TR/ TE 1701/ 32.4 msec; FOV 4 cm; matrix size 128 × 128; number of slices 4 or 8; slice thickness 3 mm. Two control images were obtained before particle administration. Nine test images were acquired every 10 minutes after addition of particles (6 and 3 during the recirculatory and nonrecirculatory perfusion modes, respectively).

Image analysis was based on SI measurements of liver parenchyma, external reference tube, and image background. Three circular ROIs were selected in liver parenchyma, and two circular ROIs were selected for background noise measurements. The ROI size and localization were unaltered during the image analysis. For each image, the SI_{liver} and SI_{noise} values were taken as the mean intensity of the ROIs. Signal-to-reference ratios (SRR), SI_{liver}/ SI_{ref}, and SNR values were calculated for test and control images. The RCE in the liver parenchyma was calculated, as previously described, using a mean value for $SRR_{control}$ and $SNR_{control}$. After termination of the perfusions, livers were weighed and freeze-stored for later ICP-AES analysis.

ICP-AES Analysis

The agar samples were digested and analyzed with respect to metal content, as previously described (11).

[1]ICP-AES analysis of filtered suspensions showed at the most a 4% loss of particulate material upon filtration.

[2]A mean liver SNR value was used for the control group as the liver SNR of control rats differed by less than 5%.

Tissue samples were dried for 24 hours at 110°C (Termaks TS 4057, Bergen, Norway). After addition of the internal standard yttrium and concentrated nitric acid, the tissues underwent a heating cycle of 210 minutes, up to 130°C (Tecator Digestion System 40 with Autostep 1012 Controller, Höganäs, Sweden). After cooling, hydrogen peroxide 30% (v/ v) was added to the tissues, which were further digested at 100°C for 30 minutes. The solutions of the digested samples were cooled and diluted to the mark with water. The metal ion concentration was determined by using a multipoint standard calibration curve (Perkin Elmer Plasma 2000 ICP-AES, Norwalk, CT) (11). The metal contents/ g of both wet and dry tissue were calculated.

Statistical Analysis

The data are given as mean values ± standard error of the mean (SEM). One-way analysis of variance was used to test for differences between control and dosage groups as well as differences in efficacy between particulate preparations. The probability *(P)* values were adjusted for multiple comparisons by the Bonferroni method (14). *P* values of less than 0.05 were considered statistically significant.

RESULTS

In Vitro Characterization

The physicochemical properties of the particulate formulations are given in Table 1. The magnetic susceptibility of the particles was independent of metal content and was approximately 1.9-fold higher for the Dy-DTPA-SP than for the Gd-DTPA-SP. For nonparticulate Gd-DTPA, r1 and r2 values of 3.9 and 4.7 s^{-1} $mmol^{-1}$ L, respectively, were obtained. The corresponding relaxivities for nonparticulate Dy-DTPA were 0.10 and 0.12 s^{-1} $mmol^{-1}$ L. Both the r1 and r2 values of Gd-DTPA-SP were about a factor of 1.6 to 2 higher than those of nonparticulate Gd-DTPA. The r1 values of Dy-DTPA-SP were approximately 1.5-fold higher than those of nonparticulate Dy-DTPA. The r2/ r1 ratio of Dy-DTPA-SP was significantly higher than that of nonparticulate Dy-DTPA, and the ratio increased with Dy content. Similar r2/ r1 ratios were obtained for the Gd-DTPA-SP preparations and nonparticulate Gd-DTPA.

Ex Vivo Tissue Relaxometry

Table 2 summarizes the effect of particles with low metal content on the relaxation times of liver, spleen, lungs, and blood. The Gd-DTPA-SP gave a dose-dependent T1 shortening in all tissues and blood throughout the dosage range ($P < 0.001$ for dosage groups versus control). Homogenization of liver further shortened T1. The T2 shortening was significant in all tissues and blood in the tested Gd dosage range ($P < 0.04$ for dosage groups versus control). No further T2 shortening was observed after liver homogenization. The Dy-DTPA-SP had no effect on the T1 and T2 in either intact or homogenized liver. A significant T1 effect was observed in spleen at all dosages of Dy-DTPA-SP ($P < 0.01$ for dosage group versus control). For blood and lungs, a marked T1 reduction was obtained at dosages of 50 µmol Dy/ kg and above ($P < 0.02$ for 50 µmol/ kg dosage groups versus control). A T2 shortening was observed in lungs, spleen and blood at dosages of 50 µmol Dy/ kg and above ($P < 0.04$ for 50 µmol/ kg dosage groups versus control). Histological examination of liver and blood samples showed the periportal distribution of particles with uptake in the liver Kupffer cells and particle internalization into polymorphonuclear leukocytes, respectively (results not shown).

In Vivo Liver Imaging

The effect of low- and high-loading particles on the in vivo liver contrast enhancement is summarized in Tables 3 and 4, respectively. On T1-w SE images, a significant dose-dependent positive RCE was observed for the low-loading Gd-DTPA-SP in the dosage range 50–150 µmol Gd/ kg (50 vs 100 µmol Gd/ kg, $P = 0.04$; 100 vs 150 µmol Gd/ kg, $P = 0.005$). The low-loading Dy-DTPA-SP reduced the liver SI on T1-w SE images at

Table 1
Physicochemical Characteristics of Gd-DTPA-SP and Dy-DTPA-SP Preparations

Particulate substance	Metal content (% w/w)	Relaxivity (s^{-1} $mmol^{-1}$ L)[a,b]			Particle diameter (µm)	Electrophoretic mobility (µm cm/V s)	Magnetic susceptibility[b,c] (10^{-2} cm^3 mol^{-1})	Experiment
		r1	r2	r2/r1				
Gd-DTPA-SP	2.7	7.6	9.3	1.2	1.5	−0.5	2.4	Tissue relaxometry/in vivo liver imaging
	4.0	7.2	9.0	1.3	2.4	−2.3	2.4	In vitro relaxometry
	6.7	6.2	8.7	1.4	2.3	−1.8	2.4	In vitro relaxometry
	8.0	6.2	7.4	1.2	2.2	−2.5	2.4	Ex vivo liver imaging
	9.3				2.7	−0.9	2.4	In vivo liver imaging
Dy-DTPA-SP	2.7	0.15	3.1	21	1.5	−0.5	4.9	Tissue relaxometry/in vivo liver imaging
	5.7	0.15	3.4	23	2.6	−1.8	4.5	In vitro relaxometry
	9.6				2.8	−2.4	4.4	Ex vivo liver imaging
	10.9				2.6	−1.1	4.5	In vivo liver imaging
	12.7	0.16	4.1	26	2.7	−1.9	4.4	In vitro relaxometry

[a](0.8% agar gel, 37°C, 0.47 T).
[b]Correlation coefficient ≥ 0.99.
[c]22°C.

Table 2
Effect of Gd-DTPA-SP and Dy-DTPA-SP With Low Metal Content (2.7% Gd or Dy) on Blood and Tissue Relaxation Times in Rats 30 Minutes After IV Administration (37°C, 0.47 T)*

Dosage (μmol Gd or Dy/kg)	Relaxation times (msec) T1 and (T2)				
	Liver	Liver, homog.	Spleen	Lungs	Blood
Control	295 ± 4	289 ± 1	573 ± 16	649 ± 13	1036 ± 17
	(49 ± 1)	(48 ± 1)	(65 ± 2)	(72 ± 2)	(316 ± 3)
Gd-DTPA-SP					
20	259 ± 1	252 ± 1	349 ± 7	502 ± 14	766 ± 17
	(45 ± 1)	(44 ± 1)	(54 ± 1)	(63 ± 4)	(274 ± 3)
50	211 ± 3	200 ± 2	190 ± 5	294 ± 13	354 ± 7
	(44 ± 1)	(43 ± 1)	(47 ± 1)	(52 ± 3)	(210 ± 13)
150	137 ± 9	104 ± 3	170 ± 2	240 ± 3	185 ± 2
	(36 ± 1)	(34 ± 1)	(37 ± 1)	(43 ± 1)	(105 ± 1)
Dy-DTPA-SP					
20	289 ± 2	287 ± 1	500 ± 7	635 ± 13	1013 ± 11
	(47 ± 1)	(49 ± 1)	(55 ± 1)	(65 ± 2)	(310 ± 2)
50	290 ± 1	287 ± 4	456 ± 14	542 ± 12	980 ± 6
	(45 ± 1)	(47 ± 1)	(52 ± 1)	(62 ± 1)	(266 ± 5)
150	287 ± 2	280 ± 2	400 ± 2	497 ± 6	829 ± 5
	(47 ± 1)	(46 ± 2)	(50 ± 1)	(60 ± 3)	(215 ± 4)

*Data are given as mean ± SEM (control: $n = 10$; test dosages: $n = 4$).

dosages of 50 μmol Dy/ kg and above. The high-loading Gd-DTPA-SP had no marked effect on the SI in T1-w SE images, and a dose-dependent negative RCE was obtained for the high-loading Dy-DTPA-SP (50 vs 100 μmol Dy/ kg, $P < 0.01$, at both time points). On the GRE images, a significant negative RCE was observed at all dosages for the particles, irrespective of metal content. The effect was dose-dependent in the 50–150 μmol Gd/ kg dosage range for the Gd-DTPA-SP with low metal content (50 vs 100 μmol Gd/ kg, $P = 0.03$; 100 vs 150 mmol Gd/ kg, $P = 0.03$). The negative RCE was also dose-dependent in the 20–100 μmol Dy/ kg dosage range for the low-loading Dy-DTPA-SP (50 vs 20 μmol Dy/ kg, $P = 0.025$; 50 vs 100 μmol Dy/ kg, $P = 0.017$). No further liver SI decrease was obtained on GRE images at a higher Dy dosage. At dosages of 50 μmol/ kg and above, the Dy-DTPA-SP with low metal content had a stronger effect on the liver SI decrease on GRE images than the corresponding Gd-DTPA-SP (Dy versus Gd 50 μmol/ kg, $P = 0.004$; 100 μmol/ kg, $P = 0.009$; 150 μmol/ kg, $P < 0.001$). A dose-dependent response was also obtained on GRE images for the high-loading Dy-DTPA-SP (50 vs 100 μmol Dy/ kg, $P < 0.05$ at both time points). No dose dependency was observed for the Gd-DTPA-SP with high metal content. At both tested dosages, the high-loading Dy-DTPA-SP were more efficient negative contrast enhancers on GRE images than the corresponding Gd-DTPA-SP (Dy versus Gd at both time points: 50 μmol/ kg, $P < 0.05$; 100 μmol/ kg, $P < 0.02$). The different TE in the GRE sequences did not allow any comparison of the liver RCE for the high- and low-loading particles.

Table 3
Effect of Gd-DTPA-SP and Dy-DTPA-SP With Low Metal Content (2.7% Gd or Dy) on Liver Contrast Enhancement in Rats 30 Minutes After IV Administration (2.4 T)*

Dosage (μmol Gd or Dy/kg)	Relative liver contrast enhancement	
	T1-w SE	GRE
Gd-DTPA-SP		
20	+0 (±3)	−29 (±3)
50	+62 (±3)	−37 (±3)
100	+76 (±2)	−56 (±3)
150	+100 (±6)	−67 (±1)
Dy-DTPA-SP		
20	−6 (±3)	−41 (±4)
50	−19 (±5)	−67 (±2)
100	−26 (±2)	−82 (±2)
150	−30 (±5)	−84 (±1)

*SE = spin echo, GRE = gradient-recalled echo. T1-w SE: TR/TE 150/12.6 msec; GRE: TR/TE/flip angle 50/14 msec/20°. Data are given as mean ± SEM ($n = 3$ in test groups; $n = 8$ in control group).

Ex Vivo Liver Imaging

Figure 2 shows the time evolution of the negative RCE in rat liver during perfusion with high-loading par-

Table 4
Effect of Gd-DTPA-SP and Dy-DTPA-SP With High Metal Content (9.3% Gd or 10.9% Dy) on Liver Contrast Enhancement in Rats (2.4 T)*

Dosage (μmol Gd or Dy/kg)	Relative liver contrast enhancement			
	T1-w SE		GRE	
	15 min	30 min	15 min	30 min
Gd-DTPA-SP				
50	+4 (±1)	+3 (±1)	−36 (±2)	−43 (±2)
100	+18 (±4)	+8 (±5)	−47 (±3)	−51 (±1)
Dy-DTPA-SP				
50	−18 (±2)	−17 (±0)	−51 (±3)	−53 (±4)
100	−31 (±2)	−35 (±1)	−70 (±3)	−70 (±2)

*SE = spin echo; GRE = gradient-recalled echo. T1-w SE: TR/TE 157/13.5 msec; GRE: TR/TE/flip angle 80/9 msec/20°. Data are given as mean ± SEM ($n = 3$ in test groups; $n = 6$ in control group).

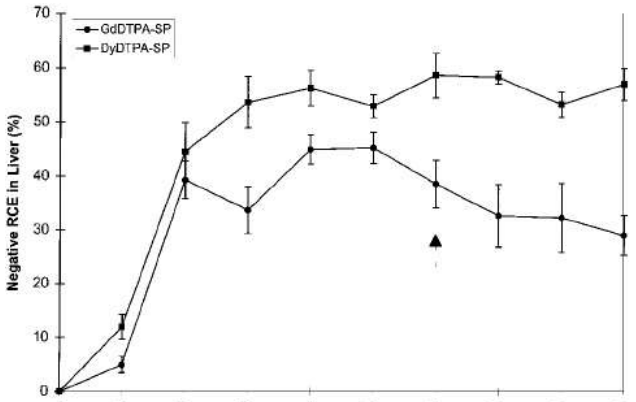

Figure 2. Contrast enhancement in the perfused rat liver after administration of Gd-DTPA-SP and Dy-DTPA-SP with high metal content (8.0% Gd or 9.6% Dy) (37°C, 4.7 T). The arrow indicates the last image acquisition during recirculatory perfusion. Data are given as mean ± SEM ($n = 3$).

ticles.[3] The contrast enhancement reached a plateau after 30 and 40 minutes of perfusion with Dy-DTPA-SP and Gd-DTPA-SP, respectively. After 60 minutes of recirculatory perfusion, the Dy-DTPA-SP had the strongest negative contrast effect with, an RCE of −59 ± 4% compared with −39 ± 4% for the Gd-DTPA-SP (Dy versus Gd, $P = 0.03$). During the last 30 minutes of nonrecirculatory perfusion, the contrast enhancement remained essentially invariant for the Dy-DTPA-SP and Gd-DTPA-SP, with final values of −57 ± 3% and -29 ± 4%, respectively (Dy versus Gd, $P = 0.004$). The ratio of the final liver RCE was 1.96, which approximated the ratio of their magnetic susceptibilities. Figure 3 shows the effect of the Dy-DTPA-SP on the SI of the perfused rat liver, 30 and 90 minutes after particle administration.

ICP-AES Tissue Analysis

Tables 5 and 6 report the tissue content and uptake of Gd and Dy after iv administration of low- and high-loading particles (in vivo liver imaging experiments). The metal content/ g dry tissue is not reported for purposes of clarity. The tissue deposition of Gd and Dy was similar and generally dose dependent. At equivalent dosages, the tissue uptake was more extensive for the high-loading particles, their liver uptake being approximately 60% higher than that of low-loading particles. The uptake of the low-loading particles in the perfused liver was similar. For the Gd-DTPA-SP, the metal content was 0.262 ± 0.028 µmol Gd/ g wet liver, and the liver uptake was 9.8 ± 1.0% of the administered dose. The corresponding values for the Dy-DTPA-SP were 0.349 ± 0.067 µmol Dy/ g wet liver and 12.0 ± 2.4%.

[3]Due to artifacts in the central part of the image (where the external reference was placed), the RCE was based on SNR values.

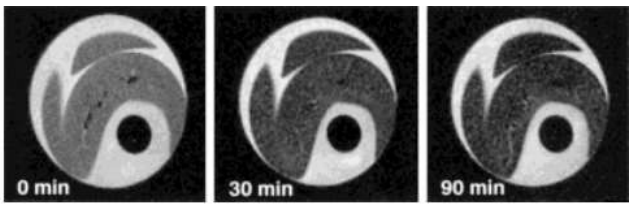

Figure 3. T2-weighted spin echo axial images of the perfused rat liver before and 30 and 90 minutes after administration of Dy-DTPA-SP with high metal content (9.6% Dy) (37°C, 4.7 T). (Please note the central position of the external reference tube).

DISCUSSION

The r1 and r2 values of the Gd-DTPA-SP are similar to those reported for several Gd-DTPA-based macromolecules, the improved relaxivity resulting from an increase in the rotational correlation time (τ_R) of the metal chelate when bound to the macromolecule, compared with free metal chelate (15,16). The low relaxivities of Dy-DTPA are due to the very short electron spin relaxation time (τ_S) of the Dy ion (17). The higher r1 values of the Dy-DTPA-SP, relative to Dy-DTPA, cannot be explained by an increase in τ_S and/ or τ_R (17) and are probably a result of the (labile) binding of water molecules to the hydrophilic starch matrix. The initial results of a more detailed investigation (18) show that the magnetic field dependence of 1/ T1 for starch particles containing no paramagnetic ions is similar to that observed for tissue and for cross-linked bovine serum albumin solutions (19,20), thereby demonstrating the existence of water molecules bound to the starch matrix. The binding of water molecules to the starch particle increase the relaxivity by two potential mecha-

Table 5
Tissue Content and Uptake of Gd and Dy 30 Minutes After IV Administration of Gd-DTPA-SP and Dy-DTPA-SP With Low Metal Content (2.7% Gd or Dy)*

Dosage (µmol Gd or Dy/kg)	Tissue content (µmol Gd or Dy/g wet tissue) (tissue uptake [% of administered dosage])		
	Liver	Spleen	Lungs
Gd-DTPA-SP			
20	0.098 ± 0.008 (24.5 ± 0.9)	0.037 ± 0.002 (0.7 ± 0.1)	0.237 ± 0.053 (10.1 ± 1.1)
50	0.242 ± 0.023 (25.3 ± 2.4)	0.180 ± 0.042 (1.2 ± 0.3)	0.843 ± 0.050 (11.8 ± 1.4)
100	0.430 ± 0.021 (23.8 ± 1.7)	0.475 ± 0.141 (1.5 ± 0.3)	1.424 ± 0.096 (9.6 ± 1.1)
150	0.633 ± 0.061 (24.3 ± 2.0)	0.421 ± 0.119 (0.9 ± 0.2)	2.360 ± 0.196 (9.7 ± 0.2)
Dy-DTPA-SP			
20	0.122 ± 0.021 (25.4 ± 1.8)	0.130 ± 0.008 (2.0 ± 0.1)	0.187 ± 0.008 (6.1 ± 0.4)
50	0.320 ± 0.047 (28.6 ± 3.8)	0.409 ± 0.013 (2.3 ± 0.3)	0.914 ± 0.045 (8.4 ± 0.1)
100	0.361 ± 0.035 (19.3 ± 1.3)	0.392 ± 0.066 (1.3 ± 0.3)	1.478 ± 0.200 (9.3 ± 1.3)
150	0.595 ± 0.051 (24.3 ± 3.4)	0.458 ± 0.142 (1.3 ± 0.6)	1.976 ± 0.278 (7.4 ± 1.1)

*Data are given as mean ± SEM ($n = 3$). The metal content/g dry tissue is not reported for purposes of clarity.

Table 6
Tissue Content and Uptake of Gd and Dy 30 Minutes After IV Administration of Gd-DTPA-SP and Dy-DTPA-SP With High Metal Content (9.3% Gd or 10.9% Dy)*

Dosage (μmol Gd or Dy/kg)	Tissue content (μmol Gd or Dy/g wet tissue) (tissue uptake [% of administered dosage])		
	Liver	Spleen	Lungs
Gd-DTPA-SP			
50	0.416 ± 0.016 (41.2 ± 1.0)	0.365 ± 0.047 (2.1 ± 0.4)	1.040 ± 0.176 (14.0 ± 1.6)
100	0.679 ± 0.047 (37.5 ± 2.0)	0.642 ± 0.049 (2.1 ± 0.2)	2.444 ± 0.302 (19.6 ± 1.1)
Dy-DTPA-SP			
50	0.363 ± 0.011 (39.5 ± 0.5)	0.297 ± 0.010 (1.8 ± 0.2)	0.765 ± 0.079 (13.2 ± 2.9)
100	0.552 ± 0.046 (34.0 ± 1.9)	0.617 ± 0.108 (1.8 ± 0.3)	1.850 ± 0.545 (17.4 ± 1.4)

*Data are given as mean ± SEM ($n = 3$). The metal content/g dry tissue is not reported for purposes of clarity.

nisms. First, water molecules could bind to the starch matrix near enough to Dy ions that there would be a significant magnetic dipolar interaction, a type of "second-sphere" effect. Secondly, and more likely, water molecules bound to the starch particle could also contribute to the increased r1 through a diamagnetic effect. The motion of particulate-bound water is sufficiently slow that the lifetime of water molecules bound to the starch matrix becomes the correlation time for the interaction, causing a large increase in the water proton relaxation rate (19,20). Cross-relaxation between water and starch protons can also contribute to this diamagnetic contribution (19,20). Because of their similarity in structure to the Dy-DTPA-SP, these two mechanisms must also exist for the Gd-DTPA-SP system. However, the intrinsic r1 of any Gd-containing species is so much larger than that of their Dy-containing counterparts that the contribution of these two additional mechanisms, if present, would be negligible.

When viewed from the outside, both the Dy-DTPA-SP and Gd-DTPA-SP can be considered a rather large magnetized particle due to the magnetization of the paramagnetic ions. Hence, a susceptibility effect, resulting from the diffusion of water protons in the outer-sphere environment of the magnetized particle, may be induced. The r2/r1 for Dy-DTPA-SP, which is higher than that of nonparticulate Dy-DTPA, shows the presence of the susceptibility effect and its dominance in comparison with the dipolar contribution. The magnetization, the magnitude of the susceptibility effects, and the r2/r1 ratio of the Dy-DTPA-SP should increase with increasing Dy content (8), as presently observed. Susceptibility effects must also exist for the Gd-DTPA-SP system, but they were not so large (compared with the dipolar contribution) as to obtain an r2/r1 ratio significantly higher than that of nonparticulate Gd-DTPA.

After intravascular administration, particulate materials are removed from the circulation by uptake into the mononuclear phagocyte system (MPS) with liver and spleen as the major clearance organs. The coating of the particles with various blood components (opsonins) enhances the uptake by MPS cells that have specific receptors for these opsonins (21). The efficiency of this opsonization process and, hence, the kinetics and degree of MPS uptake are dependent on physicochemical factors, such as the size, composition, and surface charge of the injected particles (22–24).

The relaxation time measurements of blood did not indicate a rapid clearance of the low-loading particles; the particles appeared to remain in the blood for a fairly long time, as evidenced by the significant T1 and T2 shortening of the Gd-DTPA-SP even after 30 minutes.[4] One plausible reason for the shortened relaxation times in blood would involve degradation of the particles, inasmuch as particles of this size would be expected to be rapidly and efficiently taken up by the MPS (25). Indeed, the relatively small liver uptake of the low-loading particles provided strong evidence for the hypothesis of particle degradation.[5] Two main degradation pathways have been reported for such cross-linked starch particles. The most rapid and important mechanism is the hydrolysis of the ester bond between the DTPA ligand and glucose units with release of the metal chelate (26). The second is the enzymatic cleavage by α-amylases of the glycosidic linkage between glucose units of the starch (9,27). The observed relaxation effect in blood could therefore be attributed to the presence in the circulation of particle-released Gd-DTPA and, to a lesser degree, to particulate fragments that were too small to be taken up efficiently by the MPS. The lability of the current particles was demonstrated ex vivo by particle incubation in rat blood for 2 hours (unpublished results).

The liver T1 shortening caused by the low-loading Gd-DTPA-SP cannot be attributed to particles taken up by the liver MPS. The long residence time of water molecules inside the Kupffer cell confines the T1 reduction to the intracellular water (28), which represents only a very small fraction (2%) of the total water volume in liver (29). Furthermore, most water molecules in liver could not experience the internal environment of the Kupffer cells on a time scale necessary to shorten the liver T1 because of the large distance of separation (about 75 μm) between neighboring Kupffer cells (28). Approximately 800 msec would be required for water molecules to diffuse half of that distance, and most of the tissue water could not diffuse to the Kupffer cells, even on the time scale of the intrinsic T1 of liver. The enhanced liver T1 relaxation, therefore, was mediated by Gd-DTPA-SP species (both intact and degraded) and particle-released Gd-DTPA circulating in blood. In addition, Gd-DTPA could leak into the liver interstitium and also contribute to the shortened T1. The enhanced liver T1 upon homogenization confirmed the limited dipolar relaxation in native liver, such as that reported earlier for similar Gd-DTPA-SP, Gd-based liposomes, and dex-

[4]Assuming an r1 of 5.8 s^{-1} $mmol^{-1}$ **L** [mean value of r1 for Gd-DTPA-SP (2.7% Gd) and Gd-DTPA] and a 5.4% [v/w] blood volume of the body weight [24], at least 16% of the dosage was estimated to remain in blood.
[5]Since identical particle preparations were used for tissue relaxometry and in vivo imaging experiments, the results in Table 5 were used to interpret the relaxometry data.

tran magnetite particles (30–32). However, the degree of T1 shortening was not so pronounced, which is consistent with the presence of large amounts of Gd-DTPA moieties in the extracellular space of liver.

The liver T1 effect of these low-loading Gd-DTPA-SP was reflected in a positive RCE in vivo on T1-w SE images. However, the Gd-DTPA-SP with higher metal content had no effect on the liver SI. This is consistent with a previous study reporting no ex vivo T1 effect in liver after injection of similar high-loading Gd-DTPA-SP (30). The lack of positive contrast effect in liver may be explained by a higher blood stability of the Gd-DTPA-SP with high metal content. Indeed, studies have shown that the degradation rate of the ester and glycosidic linkages in Gd-DTPA-SP decreases with increasing Gd content (9,26). Consequently, the higher stability and, possibly, the larger particle size and more negative surface charge of the high-loading Gd-DTPA-SP contributed to a higher liver uptake, compared with the low-loading analogs (Table 1), as confirmed by the ICP-AES results. Because of substantial particle localization within the Kupffer cells, there would be no positive liver contrast effect.

The confinement of paramagnetic contrast material within Kupffer cells is known to promote liver susceptibility effects (4,31,32). Such effects should be invariant with the r2 of the contrast agent and depend only on the magnetization of the Kupffer cell—the latter modulated by the field strength, magnetic susceptibility, and intracellular concentration of the agent. The Dy-DTPA-SP were expected to be more efficient susceptibility agents than the Gd-DTPA-SP, because of the higher magnetic susceptibility. However, the intracellular concentration of the Dy-DTPA-SP was not high enough to result in a magnetization that would significantly shorten the liver T2 at 0.47 T. Because the Dy-DTPA-SP showed no T2 decrease in liver, the T2 shortening induced by the Gd-DTPA-SP must be a dipolar effect resulting from particle degradation in blood, as explained previously.

Susceptibility effects in liver were expected to increase with field strength. Indeed, at 2.4 T, the GRE images of in vivo liver showed a more marked negative RCE for the Dy-DTPA-SP than did the Gd-DTPA-SP. The T2-w SE imaging results of the perfused liver model at 4.7 T complemented those obtained in vivo, because both Gd-DTPA-SP and Dy-DTPA-SP were efficient negative contrast enhancers. The onset of contrast occurred within 20 minutes, implying rapid liver uptake of the particles. The invariant RCE during the nonrecirculatory perfusion demonstrated the involvement of intracellularly located particles in the liver contrast enhancement. The twofold higher RCE for the Dy-DTPA-SP confirmed that the negative liver contrast effect was caused by the susceptibility effect, resulting from the confinement within Kupffer cells of a paramagnetic material with a higher magnetic susceptibility. It is of interest that the particle uptake in the perfused liver was lower than the in vivo liver model. This could be attributed to the lack of opsonization process, as the perfusate was a Krebs-Henseleit buffer devoid of any blood components.

The spleen also played an important role in the blood clearance of particles. Despite similar tissue Gd concentrations,[5] the effect of Gd-DTPA-SP on the T1 and T2 decrease in spleen was more pronounced than in liver. Such differences in relaxation efficacy have previously been observed for Gd-DTPA-SP preparations and were attributed to the dissimilar histological architecture of the two tissues (30). Structural features in spleen, such as a more homogeneous distribution of macrophages and larger endothelial fenestrations (2–3 μm vs 0.1 μm in liver), also allowing passage of particle fragments into the splenic tissue, may be factors that enhanced the dipolar relaxation in spleen.

The relaxation effect and high metal deposition in lungs raised some concern with respect to the safety of the starch particles. The observations could not be explained by particle uptake in the lung MPS, because the macrophages do not line the pulmonary blood vessels (33). Most likely, particle aggregation and physical entrapment in the pulmonary capillaries occurred as a large number of particles arrived to the lungs during a short time period. Such particle accumulation in the lungs has been reported for similar-size gadolinium oxide particles (2).

CONCLUSIONS

The investigated Gd-DTPA-SP and Dy-DTPA-SP functioned as susceptibility agents, reducing the liver MRI signal intensity due to compartmentalization within Kupffer cells. Because of a higher magnetic susceptibility, the Dy-DTPA-SP were the most efficient negative contrast enhancers in liver. For the Gd-DTPA-SP with high loading, an increase in liver MRI signal intensity was not observed despite a relatively high r1 in vitro. The liver T1 could not be reduced because of the small Kupffer cell volume fraction, the long water residence time within the cell, and the large distance between neighboring Kupffer cells. Although positive liver enhancement was observed for the Gd-DTPA-SP with low metal content, this effect was not caused by intact particles. Rather, it was attributed to the presence in the blood circulation of free Gd-DTPA and particulate fragments caused by particle degradation, inasmuch as starch particles with low metal content were known to be less stable than particles with a higher metal content. In addition, Gd-DTPA probably extravasated into the liver tissue, further enhancing the positive liver contrast. The potential intracellular lability of the DTPA chelate (34) and particle accumulation in lungs represented practical limitations for the use of the current paramagnetic particles as MRI contrast agents. However, the starch particles investigated are good models, which demonstrate and explain that factors other than relaxation properties must be considered to interpret differences properly between in vitro and in vivo contrast efficacy. A comprehension of these differences is critical for understanding the behavior of particulate contrast agents in vivo.

ACKNOWLEDGMENTS

The authors thank D. Grant and I. Martinsen for valuable discussions, as well as K. A. Bjerkeli, M. Arshad (all Nycomed Imaging AS, Oslo, Norway), and K. Thyberg (Department of Experimental Research, Malmø University Hospital, University of Lund, Malmø, Sweden) for providing technical assistance. S.L.F is supported by the Norwegian Research Council (contract 107462/410). J.-M.C. is supported by the ARC Program 95/00–194 of the French Community of Belgium.

REFERENCES

1. Schwendener RA. Liposomes as carriers for paramagnetic gadolinium chelates as organ specific contrast agents for magnetic resonance imaging (MRI). J Liposome Res 1994;4:837–855.
2. Burnett KR, Wolf GL, Schumacher HR Jr, Goldstein EJ. Gadolinium oxide: a prototype agent for contrast enhanced imaging of liver and spleen with magnetic resonance. Magn Reson Imaging 1985;3:65–71.
3. Braddock-Wilking J, Nosco DL, Hynes MR, Galen KP, Dorshow RB, Adams MD. Manganese hydroxylapatite as a potential MR contrast agent for liver imaging. Invest Radiol 1994;29:S251–S254.
4. Wisner ER, Merisko-Liversidge E, Kellar K, et al. Preclinical evaluation of manganese carbonate particles for magnetic resonance imaging of the liver. Acad Radiol 1995;2:140–147.
5. Saeed M, Wendland MF, Higgins CB. Contrast media for MR imaging of the heart. J Magn Reson Imaging 1994;4:269–279.
6. Moseley ME, Vexler Z, Asgari HS, et al. Comparison of Gd- and Dy-chelates for T2* contrast-enhanced imaging. Magn Reson Med 1991;22:259–264.
7. Dennie J, Sorensen AG, Weisskoff RM, et al. Hemodynamic imaging with Dy-DTPA-BMA in humans: direct comparison with Gd chelates. In: Proceedings of the 4th Annual Meeting of the International Society for Magnetic Resonance in Medicine. New York: International Society for Magnetic Resonance in Medicine; 1996. p 1716.
8. Gillis P, Koenig SH. Transverse relaxation of solvent protons induced by magnetized spheres: application to ferritin, erythrocytes and magnetite. Magn Reson Med 1987;5:323–345.
9. Rongved P, Lindberg B, Klaveness J. Cross-linked, degradable starch microspheres as carriers of paramagnetic contrast agents for magnetic resonance imaging: synthesis, degradation, and relaxation properties. Carbohydr Res 1991;214:325–330.
10. Rongved P, Klaveness J, Strande P. Starch microspheres as carriers for x-ray imaging contrast agents: synthesis and stability of new amino-acid linker derivatives. Carbohydr Res 1997;297:325–331.
11. Fossheim S, Johansson C, Fahlvik AK, Grace D, Klaveness J. Lanthanide-based susceptibility contrast agents: assessment of the magnetic properties. Magn Reson Med 1996;35:201–206.
12. Colet JM, Muller RN. Effects of opsonins on the uptake of magnetic starch microspheres by rat Kupffer cells. MAGMA 1994;2:303–305.
13. Colet JM. Study of the mechanisms of hepatic internalization of molecular and nanoparticular systems, contrast agents for magnetic resonance imaging. Ph.D. Thesis, University of Mons-Hainaut, Mons, Belgium, 1995.
14. Altman DG. In: Practical statistics for medical research. London: Chapman & Hall; 1995. p 210–212.
15. Armitage FE, Richardson DE, Li KCP. Polymeric contrast agents for magnetic resonance imaging: synthesis and characterization of gadolinium diethylenetriamine pentaacetic acid conjugated to polysaccharides. Bioconjugate Chem 1990;1:365–374.
16. Spanogue M, Lanens D, Dommisse R, Van der Linden A, Alderweireldt F. Proton relaxation enhancement by means of serum albumin and poly-L-lysine labeled with DTPA-Gd^{3+}: relaxivities as function of molecular weight and conjugation efficiency. Magn Reson Imaging 1992;10:913–917.
17. Bertini I, Capozzi F, Luchinat C, Nicastro G, Xia Z. Water proton relaxation for some lanthanide aqua ions in solution. J Phys Chem 1993;97:6351–6354.
18. Fossheim SL, Spiller M, Kellar KE. NMRD investigation of Dy-DTPA- and Gd-DTPA-labeled starch particles: selection of a suitable suspension medium and influence of the starch matrix on relaxivity. Invest Radiol (in press).
19. Koenig SH, Brown RD III, Ugolini R. A unified view of relaxation in protein solutions and tissue, including hydration and magnetization transfer. Magn Reson Med 1993;29:77–83.
20. Koenig SH, Brown RD III, Ugolini R. Magnetization transfer in cross-linked bovine serum albumin solutions at 200 MHz: a model for tissue. Magn Reson Med 1993;29:311–316.
21. Roitt IM. Innate immunity. In: Roitt IM, editor. Essential immunology. Oxford, England: Blackwell Scientific Publications; 1994. p 3–20.
22. Chouly C, Pouliquen D, Lucet I, Jeune JJ, Jallet P. Development of superparamagnetic nanoparticles for MRI: effect of particle size, charge and surface nature on biodistribution. J Microencapsulation 1996;13:245–255.
23. Harashima H, Kiwada H. Liposomal targeting and drug delivery: kinetic consideration. Adv Drug Deliv Rev 1996;19:425–444.
24. Liu D. Animal species-dependent liposome clearance. J Liposome Res 1996;6:77–97.
25. Laakso T, Smedsrød B. Cellular distribution in rat liver of intravenously administered polyacryl starch and chondroitin sulfate microparticles. Int J Pharmacol 1987;36:253–262.
26. Rongved P, Hauk Fritzell T, Strande P, Klaveness J. Polysaccharides as carriers for magnetic resonance imaging contrast agents: synthesis and stability of a new amino acid linker derivative. Carbohydr Res 1996;287:77–89.
27. Tuma RF. The use of degradable starch microspheres for transient occlusion of blood flow and for drug targeting to selected tissues. In: Davis SS, Illum L, Mc Vie J G, Tomlinson E, editors. Microspheres and drug therapy: pharmaceutical, immunological and medical aspects. Amsterdam: Elsevier; 1984. p 189–203.
28. Bacic G, Niesman MR, Magin RL, Scwartz HM. NMR and ESR study of liposome delivery of Mn^{2+} to murine liver. Magn Reson Med 1990;13:44–61.
29. Blouin A, Bolender RP, Weibel ER. Distribution of organelles and membranes between hepatocytes and nonhepatocytes in the rat liver parenchyma: a stereological study. J Cell Biol 1977;72:441–455.
30. Fahlvik AK, Holtz E, Klaveness J. Relaxation efficacy of paramagnetic and superparamagnetic microspheres in liver and spleen. Magn Reson Imaging 1990;8:363–369.
31. Fossheim SL, Colet JM, Månsson S, Fahlvik AK, Muller RN, Klaveness J. Paramagnetic liposomes as MRI contrast agents: assessment of contrast efficacy in various liver models. Invest Radiol 1999;33:810–821.
32. Magin RL, Bacic G, Niesman MR, Alameda JC Jr, Wright SM, Scwartz HM. Dextran magnetite as a liver contrast agent. Magn Reson Med 1991;20:1–16.
33. Ganong WF. Pulmonary function. In: Ganong WF, editor. Review of medical physiology. East Norwalk, CT: Apple & Lange; 1989. p 547–562.
34. Unger EC, Fritz TA, Tilcock C, New TE. Clearance of liposomal gadolinium: in vivo decomplexation. J Magn Reson Imaging 1991;1:689–693.